

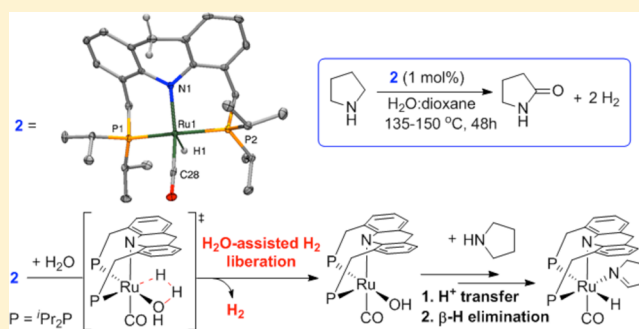
# Mechanistic Investigations of the Catalytic Formation of Lactams from Amines and Water with Liberation of H<sub>2</sub>

Urs Gellrich,<sup>†,‡</sup> Julia R. Khusnutdinova,<sup>†,§,‡</sup> Gregory M. Leitus,<sup>||</sup> and David Milstein<sup>\*,†</sup>

<sup>†</sup>Department of Organic Chemistry and <sup>||</sup>Department of Chemical Research Support, Weizmann Institute of Science, Rehovot, 76100, Israel

## Supporting Information

**ABSTRACT:** The mechanism of the unique lactam formation from amines and water with concomitant H<sub>2</sub> liberation with no added oxidant, catalyzed by a well-defined acridine-based ruthenium pincer complex was investigated in detail by both experiment and DFT calculations. The results show that a dearomatized form of the initial complex is the active catalyst. Furthermore, reversible imine formation was shown to be part of the catalytic cycle. Water is not only the oxygen atom source but also acts as a cocatalyst for the H<sub>2</sub> liberation, enabled by conformational flexibility of the acridine-based pincer ligand.



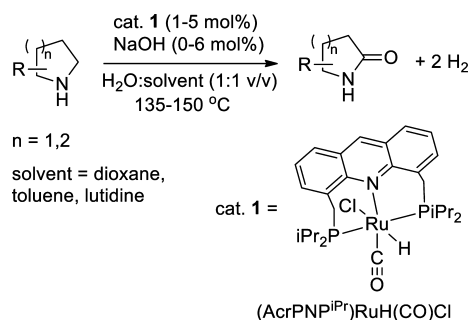
## INTRODUCTION

Amide formation is one of the most important topics in organic synthesis since this structural element is found in many pharmaceuticals and polymers. A great variety of methods have been developed for amide formation, including coupling of acylating reagents with amines, hydrolysis of nitriles, dehydrogenative coupling of amines with alcohols, and other methods.<sup>1–3</sup> However, the formation of amides via direct oxygenation of a CH<sub>2</sub> group in the  $\alpha$ -position to N remains relatively rare and typically requires the use of a stoichiometric oxidant (PhIO, peroxides, O<sub>2</sub>, RuO<sub>2</sub>/NaIO<sub>4</sub>, etc.).<sup>4–12</sup> Recently, our group has developed a fundamentally new method for lactam formation from cyclic amines using water as the only reagent and as the oxygen atom source (Scheme 1).<sup>13</sup> This transformation does not require any stoichiometric oxidant apart from water and is accompanied by liberation of H<sub>2</sub> gas, thus providing an atom economical approach for the synthesis of lactams. The lactam formation is catalyzed by the

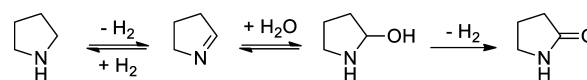
acridine-based Ru pincer complex **1** in the presence of a catalytic amount of NaOH. Complex **1** was previously developed in our group as a catalyst for alcohol amination with NH<sub>3</sub> as well as the reverse reaction, deamination of primary amines, via a “hydrogen borrowing” pathway.<sup>14–16</sup> Importantly, the lactam formation shown in Scheme 1 is conceptually different from “hydrogen borrowing” methodology, and the overall reaction is accompanied by evolution of 2 equiv of H<sub>2</sub> gas. Water plays a crucial role in this transformation acting as a source of oxygen atom for formal oxygenation of a CH<sub>2</sub> group. In principle, such transformation resembles water splitting where organic substrate (amine in this case) is used as an acceptor of O atom. The only other examples of such CH<sub>2</sub> group oxygenation by water were reported recently, and they are limited to alcohol conversion to carboxylate or CO<sub>2</sub> (in case of MeOH) in the presence of a stoichiometric base.<sup>17,18</sup> Notably, the reaction in Scheme 1 is accomplished with only a catalytic amount of a base in combination with **1** or even under base-free conditions using a modified catalyst **2** (vide infra).

We previously proposed that the amine-to-lactam conversion involves intermediate imine formation via H<sub>2</sub> liberation catalyzed by **1** (Scheme 2). Water attack would yield a hemiaminal, and a second dehydrogenation then finally results in the lactam formation.<sup>13</sup>

**Scheme 1. Lactam Formation from Cyclic Amines Using Water As the Oxygen Atom Source Catalyzed by 1**



**Scheme 2. Proposed Pathway for Lactam Formation Catalyzed by 1**



Received: February 16, 2015

Published: March 25, 2015

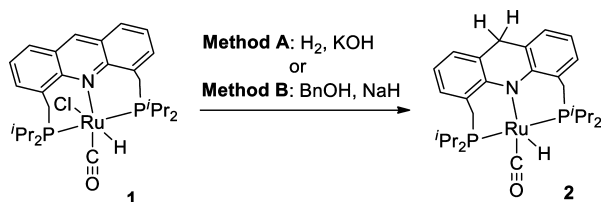
This hypothesis is in agreement with the experimental finding that H<sub>2</sub> was detected by GC/TCD after the reaction as described in a previous publication.<sup>13</sup> The imine intermediate was proposed based on the H/D exchange experiments, however, it was not observed directly under catalytic conditions. Moreover, it was proven that water acts as a source of the oxygen atom in the lactam product based on experiments using H<sub>2</sub><sup>18</sup>O.<sup>13</sup>

However, the catalytic mechanism and the role of acridine-based pincer ligand in this unprecedented amine-to-lactam dehydrogenation remained unclear. The aim of the study presented herein is to investigate the mechanism by combining experimental and theoretical investigations.

## RESULTS AND DISCUSSION

**Role of a Base and Transformation of the Ligand during Catalysis.** Previous studies involving complex **1** reported by our group indicate that the acridine-based pincer ligand exhibits reactivity at C9 position of the acridine backbone, leading to reduction of the central acridine ring.<sup>19</sup> In particular, it was previously shown that complex **1** reacts with H<sub>2</sub> in the presence of a base to give a hydrido carbonyl complex **2** (Scheme 3, Method A) in which a central acridine ring is reduced.<sup>19</sup> Complex **2** was previously isolated and fully characterized by NMR, IR spectroscopy, and elemental analysis.<sup>19</sup>

### Scheme 3. Synthesis of the Dearomatized Hydride Carbonyl Complex **2**<sup>a</sup>



<sup>a</sup>Method A (ref 17): H<sub>2</sub> (5 bar), KOH (1 equiv), toluene, 135 °C, 48 h. Method B: benzyl alcohol (3.3 equiv), NaH (12 equiv), toluene, RT, 2 h.

In addition, Hofmann et al. recently reported the synthesis of Ru complexes with an analogous acridine-based pincer ligand bearing bis(cyclohexyl)phosphine donors instead of bis(isopropyl)phosphine donors and their reactivity in amination of alcohols with NH<sub>3</sub>.<sup>20</sup> They showed that the reaction of the analogous (AcrPNP<sup>Cy</sup>)RuH(CO)Cl complex with benzyl alcohol in the presence of a base also leads to the reduction of the central acridine ring accompanied by benzyl alcohol dehydrogenation.<sup>20</sup>

We hypothesized that the acridine-based ligand AcrPNP<sup>Pr</sup> could undergo a similar reduction during the reaction with amines or alcohols and synthesized complex **2** according to the modified procedure reported by Hofmann et al. (Scheme 3, Method B), by the reaction with benzyl alcohol (or ethanol) in the presence of NaH. The same complex can also be obtained when <sup>t</sup>BuOK is used as a base. Complex **2** was isolated in 77% yield and characterized by <sup>1</sup>H, <sup>13</sup>C, and 2D NMR. Single crystals of **2** were grown by slow evaporation of pentane solution and were characterized by X-ray diffraction (Figure 1).<sup>21</sup>

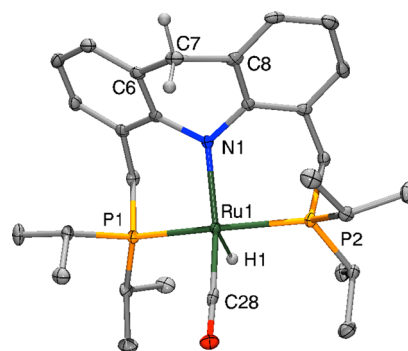


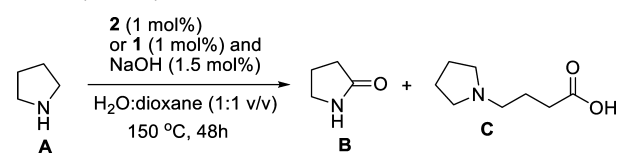
**Figure 1.** ORTEP representation of **2** (50% probability ellipsoids). Selected bond lengths (Å) and angles (deg): Ru1–N1 2.124(2), Ru1–P1 2.3301(9), Ru1–P2 2.324(1), Ru1–C28 1.816(4), Ru1–H1 1.47(4), C7–C6 1.502(5), C7–C8 1.502(5); P1–Ru1–P2 160.55(3), N1–Ru1–C28 154.93(13), C6–C7–C8 108.1(3).

The X-ray structure of **2** reveals a distorted square pyramidal Ru<sup>II</sup> center bound to a pincer ligand through two P atoms and an acridine N atom. It unambiguously confirms that the central acridine ring is reduced: the bond distances C7–C6 and C7–C8 at the central acridine ring are typical for single C–C bonds, and the bond angle C6–C7–C8 is characteristic of a tetrahedral sp<sup>3</sup> hybridized central carbon. The hydrogen atom H1 was localized as an electron density peak (see Experimental Details section). No ligands are present trans to the hydride, likely due to its strong trans influence. The Ru–N bond distance (2.124 Å) is significantly shorter than the Ru–N distance reported for complex **1** (2.479 Å), suggesting that the reduction of the central acridine ring leads to a stronger interaction between the Ru center and a negatively charged N donor.<sup>15,19</sup> Moreover, the X-ray structure is in good agreement with the DFT-calculated structure for **2** (*vide infra*).

We then tested the catalytic activity of complex **2** in the absence of a base in amine-to-lactam conversion under the conditions that were previously reported for catalyst **1** in the presence of catalytic NaOH, using pyrrolidine (**A**) as a model substrate. When pyrrolidine was heated in a dioxane-water mixture (1:1 v/v) in the presence of 1 mol % of **2** at 150 °C for 48 h, 2-pyrrolidone (**B**) was obtained as a major product in 55% yield. The major byproduct was 4-(1-pyrrolidinyl)butanoic acid (**C**) formed in 10% yield, similar to the results reported previously.<sup>13</sup> The comparison of these results with the analogous reaction in the presence of complex **1** (1 mol %) and NaOH (1.5 mol %) is given in Table 1 and shows that the conversion and the product yields are similar in these two systems. This result suggests that complex **2** may be the catalytically competent species under the catalytic conditions which is also consistent with our DFT study (*vide infra*).

Importantly, the catalytic activity of complex **2** was observed in the absence of NaOH suggesting that a base is not required for amine-to-lactam conversion. The role of NaOH in the lactam formation catalyzed by **1** is most likely to promote the formation of the catalytically active species **2**. The possible mechanism of the formation of **2** was studied by DFT and will be discussed in more detail in the following sections.

The mass balance in entries 1 and 2 of Table 1 sums up to 99–99.5%, taking into account that the formation of **C** consumes 2 equiv of pyrrolidine **A**, thus indicating that no other significant side reactions occur under these conditions. The possible pathways leading to **C** were discussed in a previous publication.<sup>13</sup>

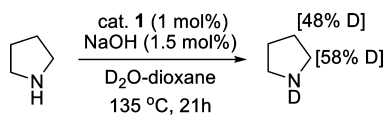
**Table 1. Reactivity of Pyrrolidine in Water-Dioxane (1:1 v/v) Catalyzed by 2 and 1/NaOH**


entry	catalyst	T, °C	conv. of A (%)	B, % yield	C, % yield
1 <sup>a</sup>	2 (1 mol %)	150	76	55	10
2 <sup>a,b</sup>	1 (1 mol %) NaOH (1.5 mol %)	150	78.5	59	9.5
3	2 (1 mol %)	135	75	64	5
4	1 (1 mol %) NaOH (1.5 mol %)	135	42.5	35	4

<sup>a</sup>Pyrrolidine (1 mmol), catalyst 2 (1 mol %) or 1 (1.0 mol %)/NaOH (1.5 mol %), water (1.5 mL), and dioxane (1.5 mL) were heated in a 50 mL thick wall pressure tube for 48 h at 150 °C (silicon oil bath temperature), if not indicated otherwise. % NMR yields and conversions were determined by NMR and reported as averages of two runs. <sup>b</sup>from ref.<sup>13</sup>

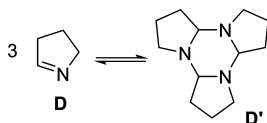
Interestingly, complex 2 also shows catalytic activity at a lower temperature, 135 °C, yielding 2-pyrrolidone in a slightly higher yield, likely due to a slower side reaction leading to the formation of C, which was formed in only 5% yield (entry 3). By comparison, complex 1 in combination with NaOH shows only moderate catalytic activity at this temperature (entry 4).

**Imine Reactivity under the Catalytic Conditions.** We have previously proposed that the amine-to-lactam conversion likely occurs through an imine intermediate (Scheme 2).<sup>13</sup> Since an imine could not be detected among the reaction products, its formation was deduced based on an H/D exchange experiment showing that significant H/D incorporation in the  $\alpha$ - as well as the  $\beta$ -positions occurs when pyrrolidine is heated in D<sub>2</sub>O-dioxane in the presence of 1/NaOH at 135 °C (Scheme 4), while only a trace amount of 2-

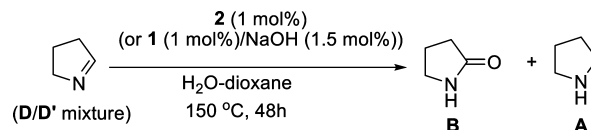
**Scheme 4. Deuterium Incorporation in the  $\alpha$ - and  $\beta$ -Position of Pyrrolidine**

pyrrolidone was formed at this temperature as reported previously.<sup>13</sup> This is consistent with reversible dehydrogenation of pyrrolidine to form 1-pyrroline (D) in the presence of the Ru catalyst that occurs before the rate limiting step.

To confirm that 1-pyrroline (D) is indeed a viable intermediate in the lactam formation, we synthesized it. 1-pyrroline is known to exist in an equilibrium mixture with the trimer D' in solution (Scheme 5),<sup>22</sup> and previous studies

**Scheme 5. Monomer–Trimer Equilibrium in a Solution of 1-Pyrroline**

demonstrated that the trimer and monomer interconvert easily in solution and cannot be separated.<sup>22</sup> Therefore, this substrate was used under standard catalytic conditions as a mixture of the monomer and trimer in a water-dioxane solution (Scheme 6).

**Scheme 6. Catalytic Experiments Using 1-pyrroline As a Substrate**

These experiments showed that independently from the applied catalytic system (1/NaOH or 2), 2-pyrrolidone was formed in yields similar to those obtained using pyrrolidine A as a substrate (Table 2 vs Table 1). These results are consistent

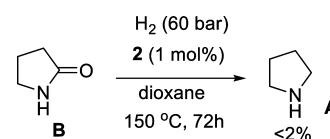
**Table 2. Conversion of Imine D to Lactam under Standard Catalytic Conditions<sup>a</sup>**

entry	catalyst	conv. of D/D' (%)	B, % yield	A, % yield
1	1/NaOH	>99	50	11
2	2	>99	55	13

<sup>a</sup>Reaction conditions: pyrroline D/D' (1 mmol), catalyst 1 (1.0 mol %)/NaOH (1.5 mol %) or 2 (1.0 mol %), and H<sub>2</sub>O-dioxane 1:1 v/v, 150 °C, 48 h. Yields and conversions were determined by NMR.

with imine D being part of the catalytic cycle. Furthermore, the formation of pyrrolidine A was observed, likely formed via hydrogenation of D with the H<sub>2</sub> evolved in the conversion of imine D to lactam B. This finding proves the assumption made so far based on the H/D exchange experiments, that the imine formation is reversible under the catalytic conditions and that imine D is a viable intermediate of the lactam formation.

**Possibility of the Reverse Reaction of Lactam-to-Amine Conversion.** To determine whether under anhydrous reaction conditions and under high pressure of H<sub>2</sub> we can achieve the reverse transformation, hydrogenation of lactams to cyclic amines, we examined the possibility of hydrogenation of 2-pyrrolidone to pyrrolidine catalyzed by complex 2. When 2-pyrrolidone was heated in anhydrous dioxane in the presence of 1 mol % of 2 under 60 bar of H<sub>2</sub>, only a trace amount of pyrrolidine was detected in the reaction mixture after 72 h at 150 °C (Scheme 7). Similarly, attempted hydrogenation of 2-

**Scheme 7. Attempted Hydrogenation of 2-Pyrrolidone to Pyrrolidine**

pyrrolidone catalyzed by 1/NaOH in water-dioxane failed to produce pyrrolidine.<sup>13</sup> This suggests that the reverse reaction likely has a high activation barrier, and the lactam formation is practically irreversible under standard catalytic conditions even in a closed system. This is fully consistent with the DFT studies as discussed below.

**Computational Investigations.** In order to gain more insights into the elementary steps of the catalytic transformation, we performed DFT calculations at the DSD-

PBEB95-D3BJ/def2-TZVPP//BP86-D3/def2-SV(P) level of theory. In order to validate the level of theory used for the geometry optimizations, we compared the structure of **2** derived from X-ray with the computed one, showing a good agreement between experimental and computed bond lengths and angles (Table 3).

**Table 3. Structural Parameters of **2** Measured by X-ray and Computed by DFT**

	X-ray	BP86-D3/def2-SV(P)
Ru–N [Å]	2.124(2)	2.136
Ru–CO [Å]	1.817(4)	1.832
Ru–P [Å] <sup>a</sup>	2.327	2.326
N–Ru–CO [deg]	154.93(13)	151.01
P–Ru–P [deg]	160.55(3)	158.81

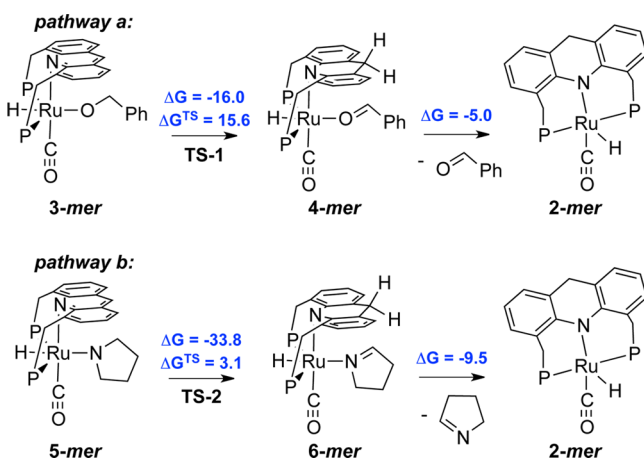
<sup>a</sup>Average over the two bond lengths.

The DSD-PBEB95-D3BJ/def2-TZVPP level of theory, chosen for the single point energy calculations, was recently shown to yield results very close to explicitly correlated coupled cluster benchmark calculations for reaction energies and barriers involving late transition-metal complexes with pincer ligands.<sup>23</sup> To take the influence of the solvent into account, the SMD model was applied for a 1:1 mixture of dioxane/water, with a dielectric constant of  $\epsilon = 40.28$ , being the average weight of dioxane and water.

**Formation of **2** and Isomerization Pathways.** Since **2** was shown to be the active catalyst, we first calculated a pathway for its formation under the conditions used for the direct synthesis (Scheme 3, Method B) and under catalytic conditions. We assumed that in the presence of NaH, the benzyl alcohol used in the synthesis of **2** gets deprotonated, and the alkoxide substitutes the chloride leading to **3-mer** (Scheme 8).

A  $\beta$ -hydride transfer to the C9 position of the acridine ring with a barrier of 15.6 kcal/mol leads to the reduced species **4-mer**. Dissociation of the formed benzaldehyde yields **2-mer** (Scheme 8, pathway a). This dearomatization mechanism via direct  $\beta$ -hydride transfer from the coordinated alkoxide to the

**Scheme 8. Formation of **2** Using Benzyl Alcohol and NaH (pathway a) or Pyrrolidine (pathway b) under Catalytic Conditions<sup>a</sup>**



<sup>a</sup>Calculated free energies (kcal/mol).

acridine ring is similar to that calculated by Hofmann et al. for the reaction of analogous complex (AcrPNP<sup>Cy</sup>)RuH(CO)Cl with MeOH.

Under catalytic conditions the pyrrolidine can displace the chloride and be deprotonated by NaOH (either simultaneously or consecutively). A  $\beta$ -hydride transfer from the deprotonated pyrrolidine ligand to the C9 of central acridine ring with a low barrier of 3.1 kcal/mol then leads to the active catalyst **2-mer** after dissociation of 1-pyrroline (pathway b) (see Figure 2). In both pathways formation of the reduced complexes **4-mer** and **6-mer** is exothermic.

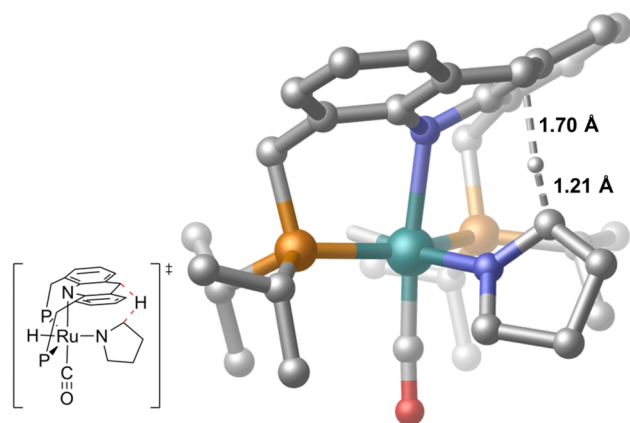
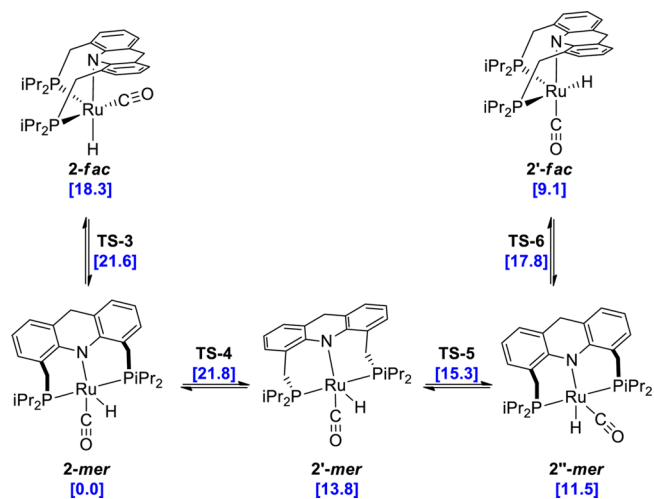


**Figure 2. TS-2** involving hydride transfer from coordinated pyrrolidine to the C9 position of the acridine ring, leading to imine dissociation and formation of the active catalyst **2-mer**. Bond lengths are given in angstrom.

We then focused on possible stereoisomers of **2** and the isomerization pathway connecting them (Scheme 9). We

**Scheme 9. Isomerization Pathway Connecting Different Conformers of **2**<sup>a</sup>**



<sup>a</sup>Calculated free energies (kcal/mol) in brackets with respect to **2-mer**.

assumed that the dearomatized acridine-based pincer ligand with the reduced central ring is sufficiently flexible to adopt both meridional and facial coordination modes in Ru complexes. In particular, some complexes with a *fac*-coordinated reduced ligand were reported previously by our group.<sup>15,19</sup> Starting from **2-fac**, **2-mer** is accessible via TS-3 with

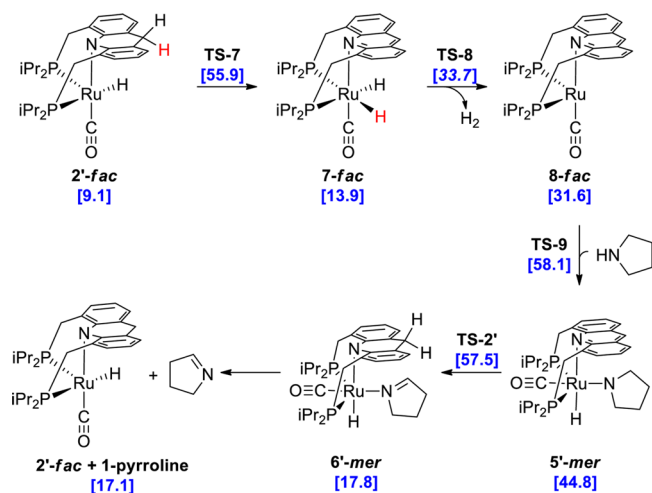


a low barrier of 3.3 kcal/mol. This conformer is predicted to be the most stable and indeed the one found by X-ray analysis. A flip of the acridine ring yields *2'-mer*. This ring flip shows the highest single barrier calculated in the isomerization pathway (21.8 kcal/mol). A change in the position of the CO and the hydride ligand yields *2''-mer*, which can directly interconvert to *2'-fac*. For the most stable *mer* conformer *2-mer* and the most stable *fac* conformer *2'-fac*, we also investigated the effect of pyrrolidine coordination to these complexes.

The free energy differences and the barriers between all conformers shown in Scheme 9 are small enough to make all conformers of **2** accessible at a reaction temperature of 150 °C. Therefore, all of them can serve as potential active catalysts.

**H<sub>2</sub> Liberation Pathways and Insights into the Role of Water in H<sub>2</sub> Elimination.** Catalytic pathways starting from *2'-fac* will now be discussed in detail, focusing on a possible explanation for the experimentally observed H<sub>2</sub> liberation. We first computed a pathway in which a hydride is transferred from the C9 position of the acridine ligand to the ruthenium (TS-7), forming the cis hydride species *7-fac*. H<sub>2</sub> elimination via TS-8 with an estimated energy of 33.7 kcal/mol yields the ruthenium(0) species *8-fac* with a free coordination site, able to undergo an oxidative insertion in the NH bond of pyrrolidine.<sup>24</sup> A proton transfer from the β position of the heterocycle in *5'-mer* and dissociation of the imine from *6'-mer* regenerates *2'-fac* (Scheme 10).

#### Scheme 10. H<sub>2</sub> Elimination and Imine Formation via a Ruthenium(0) Intermediate<sup>a</sup>



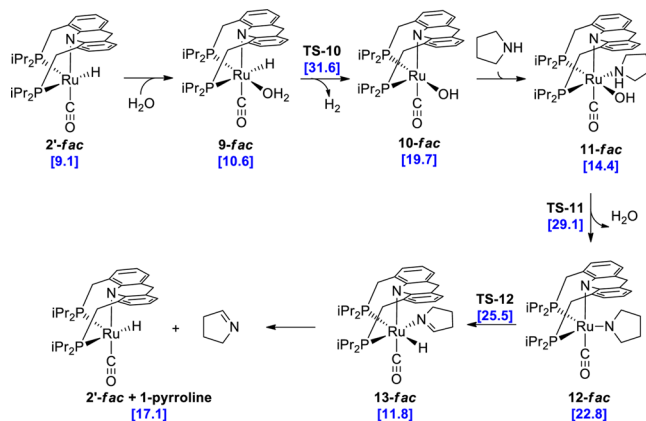
<sup>a</sup>Calculated free energies (kcal/mol) in brackets with respect to *2-mer*.

The activation energy required for the hydride transfer (TS-7) from the ring to the ruthenium and the high energy of TS-9 and TS-2' relative to *2-mer* render this mechanistic scenario unlikely even at high reaction temperatures. Since previous studies on related ruthenium pincer complexes highlighted the importance of water as proton shuttle, we investigated if water could significantly lower the activation energy required for the liberation of hydrogen.<sup>25,26</sup> Transition states in which water acts as a proton shuttle for the direct formation of *7-fac* by “bridging” Ru–H and the C9 position of the acridine with one or two molecules of water were calculated to be even higher in energy than the transition state for the hydride transfer from

the C9 position to the ruthenium (see Supporting Information for more detail).

Interestingly, we found that after coordination of a water molecule to *2'-fac*, H<sub>2</sub> elimination involving the hydride bound to the ruthenium and a proton of the water molecule can take place via a significantly lower barrier of 31.6 kcal/mol (TS-10 in Scheme 11; see also Figure 3) with respect to *2-mer*. The

#### Scheme 11. Imine Formation via H<sub>2</sub> Elimination from the Hydroxy Complex *10-fac*<sup>a</sup>



<sup>a</sup>Calculated free energies (kcal/mol) in brackets with respect to *2-mer*.

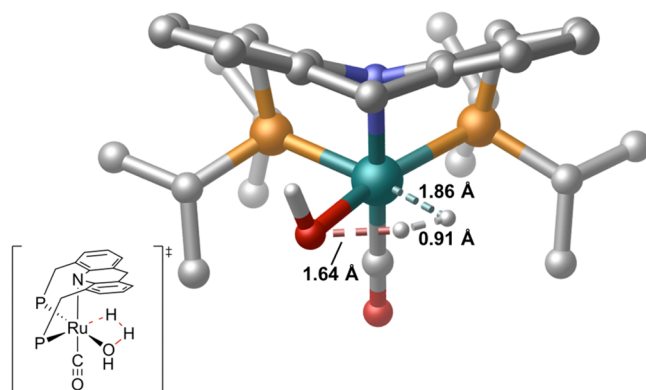


**Figure 3.** Transition state TS-10 for H<sub>2</sub> elimination from the aqua complex *10-fac*. Bond lengths are given in angstrom.

calculated Mulliken atomic charge of the hydrogen bound to water and involved in this process rises from 0.266 to 0.281 e upon coordination of the water to *2'-fac*, rendering it more protic.

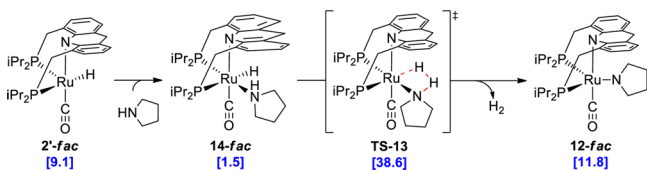
Coordination of pyrrolidine to the hydroxy complex *10-fac* yields the complex *11-fac* in which a N–H···O hydrogen bond between the pyrrolidine ligand and the hydroxyl ligand is already present. A proton transfer with concomitant H<sub>2</sub>O liberation (TS-11) results in the formation of *12-fac*. A similar transition state in the alcohol-assisted coordinated amide protonation was previously reported in the course of the investigation of the ruthenium–acridine complex catalyzed amination of primary alcohols.<sup>20</sup> The vacant coordination site in this complex renders a β-hydride elimination from the deprotonated pyrrolidine possible, resulting after dissociation in the formation of the imine and the regeneration of *2'-fac*. The actual barrier for the imine formation via the pathway depicted in Scheme 11 is 31.6 kcal/mol with respect to *2-mer*. The H/D exchange in the α-CH<sub>2</sub> group of pyrrolidine observed in D<sub>2</sub>O-

dioxane (Scheme 4) is consistent with a reversible pyrrolidine-to-(1-pyrroline) dehydrogenation and can be explained by H/D exchange of the Ru–H in complex **2** (either as **2'-fac** or **2-mer** conformer) or **13-fac** with D<sub>2</sub>O and then reinsertion of 1-pyrroline into Ru–D bond (Scheme 11). The possible pathways for H/D exchange in  $\beta$ -CH<sub>2</sub> position of pyrrolidine were discussed in a previous publication.<sup>13</sup>

The possibility of inner sphere H<sub>2</sub>O-assisted hydrogen liberation from a similar ruthenium complex was discussed previously by Yoshizawa et al. but was found to be unlikely due to high barriers required for the loss of CO ligand that enables *cis*-arrangement of Ru–H and R–OH<sub>2</sub> ligands.<sup>25</sup> Suresh et al. considered an alternative mechanism via rearrangement of a CH<sub>2</sub>-arm-deprotonated (*mer*-PNN)Ru species to allow for *cis*-arrangement of Ru–H and Ru–OH<sub>2</sub>.<sup>27</sup> In most complexes considered so far, the H<sub>2</sub>O-assisted hydrogen liberation takes place via an outer sphere mechanism (either via external attack or water molecule bridging the deprotonated arm) or the H<sub>2</sub>O molecule has first to replace a ligand, while PNN ligand remains coordinated in a *mer*-fashion.<sup>25,28,29</sup> By contrast, we believe that the mechanism of H<sub>2</sub> elimination through transition state **TS-10** is enabled by conformational *mer/fac* flexibility of the reduced AcrPNP<sup>Pr</sup> ligand allowing for coordination of water *cis* to a hydride. This is a unique feature of the acridine-based pincer ligand system compared to the “classical” pyridine-based PNN and PNP ligand motifs in which *fac*-coordination is not accessible, however, different modes of H<sub>2</sub> elimination are possible through deprotonation of the CH<sub>2</sub> arm. In addition, such conformational flexibility likely enables  $\beta$ -hydride elimination pathway leading to **10-fac**.

An alternative pathway, in which the H<sub>2</sub> elimination involves the pyrrolidine rather than water was also investigated (Scheme 12).

#### Scheme 12. H<sub>2</sub> Elimination Involving the Pyrrolidine Instead of Water As Proton Source<sup>a</sup>



<sup>a</sup>Calculated free energies (kcal/mol) in brackets with respect to **2-mer**.

The coordination of pyrrolidine to **2'-fac** is energetically preferred compared to the coordination of water. However, the barrier for H<sub>2</sub> elimination from the pyrrolidine complex **14-fac** (37 kcal/mol) is 16 kcal/mol higher than starting from the aqua complex **9-fac**. Both findings may reflect the higher basicity of pyrrolidine compared to water. The three mechanistic scenarios depicted in Schemes 10, 11, and 12 are summarized as potential free energy surface in Figure 4, indicating that the pathway involving water (Scheme 11) is the most favorable.

Formation of the imine is endothermic, in agreement with the experimental finding that the imine cannot be observed under typical reaction conditions. The barrier for the backward reaction, yielding the pyrrolidine, is smaller, which is consistent with the deuterium-labeling experiments, showing that the imine formation is reversible. However, under the actual reaction conditions using a 1:1 mixture of dioxane and water as

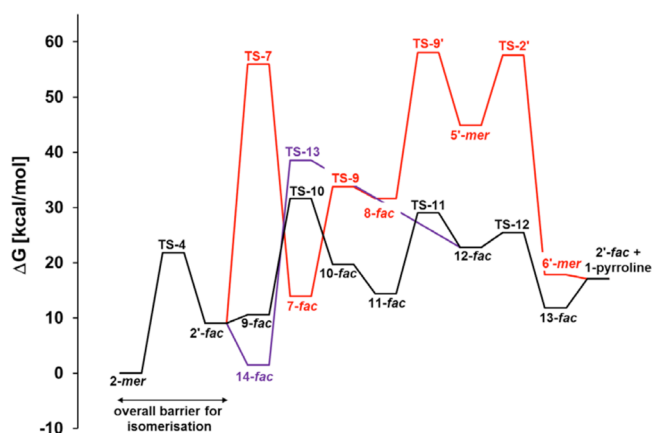
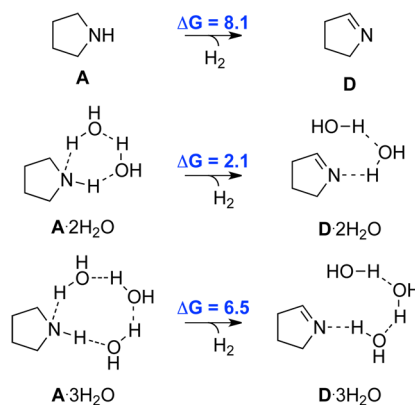


**Figure 4.** Pathways of pyrrolidine dehydrogenation involving (a) hydride transfer from the C9 position of the ligand (red); (b) H<sub>2</sub> elimination from the aqua complex **10-fac** (black); or (c) H<sub>2</sub> elimination from the pyrrolidine complex **7'-fac** (purple).

solvent, it is likely that the pyrrolidine as well as the imine form hydrogen bonds to surrounding water molecules. We therefore investigated if this affects the free energy associated with the imine formation.

Interestingly, the explicit solvation by hydrogen bonds (A·2H<sub>2</sub>O, Scheme 13) significantly lowers the endothermicity of

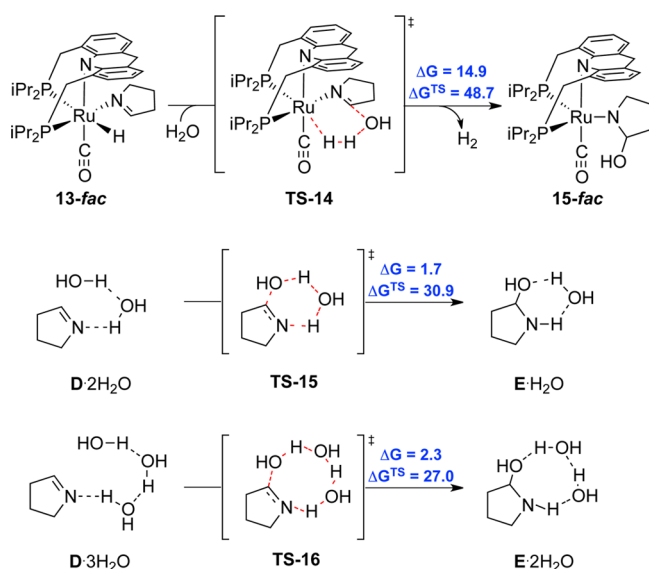
#### Scheme 13. Free Energies of the 1-pyrroline (D) Formation<sup>a</sup>



<sup>a</sup>Calculated free energies (kcal/mol).

the imine formation (by 6 kcal/mol). The effect is less pronounced with three surrounding water molecules. The reaction is furthermore driven in the direction of the imine by H<sub>2</sub> leaving the condensed phase, which is not reflected by the DFT calculations.

**Formation of a Hemiaminal and a Lactam.** The next step involves the hemiaminal formation by a nucleophilic attack of water at the imine. Coordination of the imine to ruthenium may render the imine more electrophilic and therefore facilitate this step. We were able to locate a transition state for the nucleophilic attack of water at the double bond of the imine of **13-fac** (Scheme 14, top). This transition state involves the direct elimination of H<sub>2</sub> according to IRC calculations. However, the computed barrier of 48.7 kcal/mol renders this transition state unlikely to be part of the catalytic transformation. An attack of water on the liberated imine in which a second water molecule serves as proton shuttle is more likely,

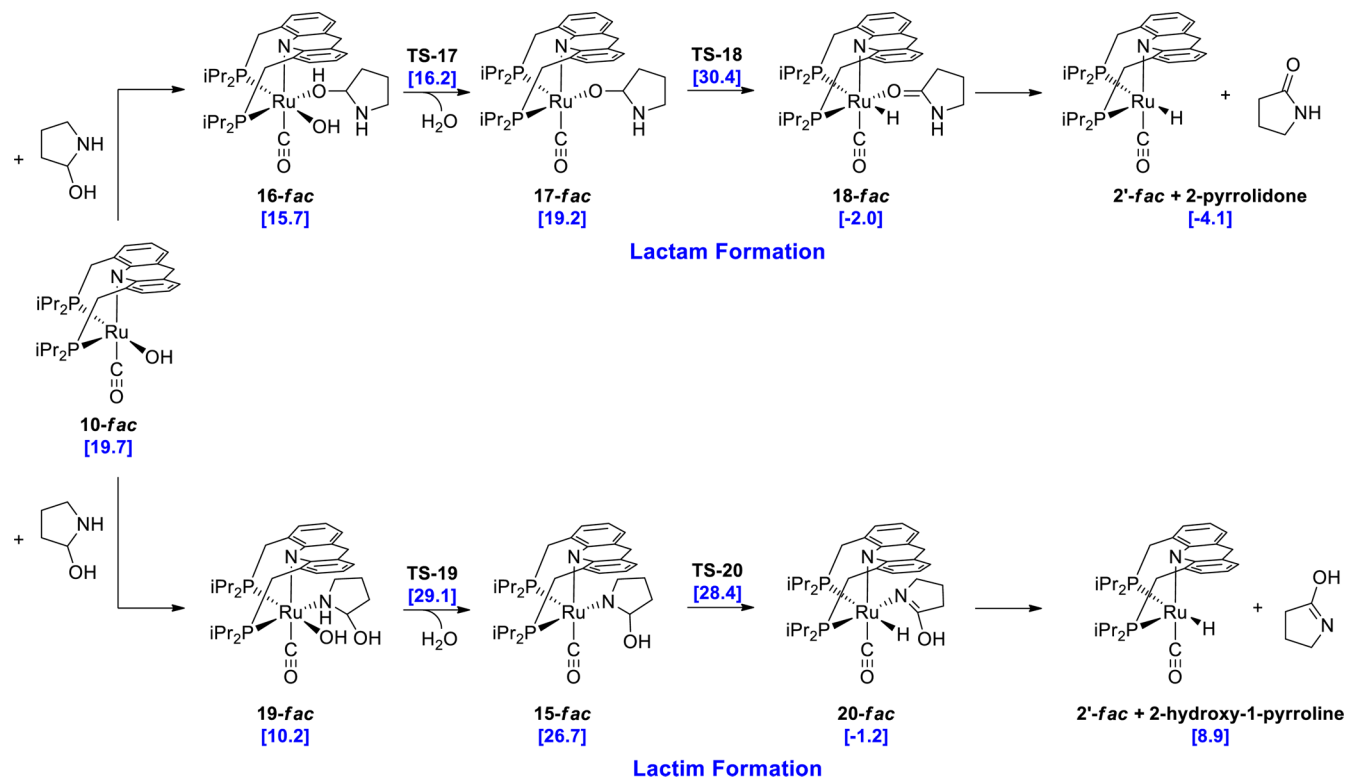
Scheme 14. Inner- and Outersphere Pathways for the Hemiaminal Formation<sup>a</sup><sup>a</sup>Calculated free energies (kcal/mol)

having a barrier of 30.9 kcal/mol (Scheme 14, bottom). An additional water molecule lowers this barrier to 27.0 kcal/mol.

Nevertheless, by taking into account that the imine formation is endothermic, the hemiaminal formation represents the rate-determining step of the catalytic transformation with an overall barrier of 33.0 kcal/mol via TS-15 and 33.5 kcal/mol via TS-16, depending if one or two water molecules assist the hemiaminal

formation. This is in agreement with the deuterium-labeling experiments which indicate that the dehydrogenation of the pyrrolidine occurs prior to the rate limiting step. Once the hemiaminal is formed, the dehydrogenation can take place in a similar manner as the dehydrogenation of the pyrrolidine. Starting from the hydroxy complex **10-fac** N-coordination of the hemiaminal is energetically favored compared to O-coordination (Scheme 15). On the other side, the proton transfer process with concomitant H<sub>2</sub>O elimination involving the OH group (TS-17) of the hemiaminal shows a lower barrier than proton transfer from the NH group (TS-19), which is in line with the acidity of these groups. The activation energy for the β-hydride elimination is lower starting from the N-coordinated complex **15-fac**. Dissociation of the O- or N-coordinated complexes **18-fac** and **20-fac** yields the lactam or lactim, respectively (Scheme 14). The pathways for the lactim and the lactam formation are summarized in Figure 5. The highest barrier for the lactim formation would be the proton transfer from the NH to the hydroxyl group bound to the ruthenium (TS-19), whereas the β-hydride elimination to form the lactam (TS-18) represents the highest barrier for the direct lactam formation. Both mechanistic scenarios seem realistic at the reaction temperature of 150 °C. The lactam is computed to be 13.0 kcal/mol more stable than the lactim, which shows that the driving force for the catalytic cycle is indeed the formation of the lactam.

Furthermore, once the hemiaminal is formed, the barrier for the forward reaction is significantly lower than the barrier for the backward reaction, explaining the observed irreversibility of the overall transformation.

Scheme 15. Pathways for the Lactam and Lactim Formation Starting with the Hydroxy Complex **10-fac**<sup>a</sup><sup>a</sup>Calculated free energies (kcal/mol) in brackets with respect to **2-mer**.

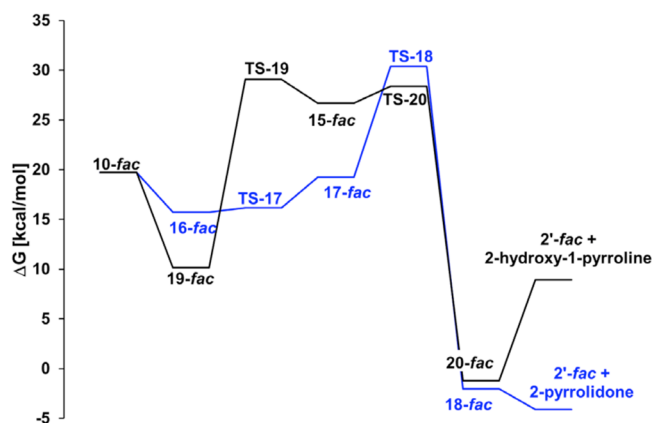


**Figure 5.** Pathways for the lactam formation (blue) and the lactim formation (black). All energies are given with respect to *2-mer*.

## CONCLUSION

In summary, we have presented herein a thorough mechanistic study of the acridine-based ruthenium pincer complex catalyzed formation of lactams from amines using water with no added oxidant. The conclusions drawn from the DFT calculations agree well with the experimental findings. Complex **2** with the reduced central ring of the acridine system was shown to be the actual catalyst, which is in agreement with the DFT computations. The isolated complex **2** is catalytically active in the pyrrolidine-to-pyrrolidone conversion even in the absence of a base, showing that catalytic NaOH that was used previously in combination with the catalyst precursor **1** is not required for the lactam formation, once the active catalyst is formed. The conformer *2-mer* was predicted to be most stable and was indeed the conformer observed by X-ray diffraction. The computations revealed that the imine formation is endothermic and proceeds with an overall small barrier, which is in agreement with the deuterium-labeling experiments and the observed reactivity of the imine under catalytic conditions. Finally, the DFT computations have shown that water might catalyze the H<sub>2</sub> liberation in a rare fashion, enabled by conformational flexibility of the reduced AcrPNP<sup>Pr</sup> ligand that allows for its *fac*-coordination. The results presented in this study might be useful for the development of other atom economic amide formations as well as the discovery of new catalytic reactions involving water as oxidant with H<sub>2</sub> liberation.

## EXPERIMENTAL DETAILS

**General Specifications.** All manipulations were carried out under a nitrogen atmosphere using standard Schlenk and glovebox techniques if not indicated otherwise. All chemicals for which synthesis is not given were commercially available from Aldrich, Acros, or STREM and were used as received without further purification. 1,4-Dioxane and toluene were purified prior to use by refluxing and distilling over Na/benzophenone under an argon atmosphere. Distilled water was purchased from Aldrich (HPLC grade) and was degassed prior to use by bubbling argon for at least 20 min. 4,5-Bis(di-iso-propylphosphinomethyl)acridine (AcrPNP) and (AcrPNP)RuH(CO)Cl (**1**) were prepared according to the literature procedures.<sup>14</sup> NMR spectra were recorded on a Avance III – 300 Bruker or AV-500 Bruker Avance spectrometer. Chemical shifts are referenced to TMS or to residual solvent resonance peaks (HDO peak at 4.79 ppm in D<sub>2</sub>O).<sup>30</sup> Mass spectra were recorded on Micromass Platform LCZ 4000, using electrospray ionization (ESI) mode. GC-MS was carried out on HP 6890 (flame ionization detector and thermal conductivity detector) and HP 5973 (MS detector)

instruments equipped with a 30 m column (Restek SMS, 0.32 mm internal diameter) with a 5% phenylmethylsilicone coating (0.25 mm) and helium as carrier gas.

**Synthesis of 2.** Sodium hydride (29.7 mg, 1.24 mmol, 12 equiv) was added to a stirred solution of **1** (62.2 mg, 0.103 mmol) and benzyl alcohol (37.0 mg, 3.3 equiv) in toluene (7 mL). The reaction mixture was stirred for 2 h at RT and then filtered through a Celite plug. The resulting orange toluene solution was evaporated to dryness, and the solid residue was washed with pentane several times to remove benzyl benzoate and excess benzyl alcohol. The resulting orange powder was dried under high vacuum for several hours. Yield 45.5 mg (0.0796 mmol, 77%). X-ray quality crystals were obtained by slow evaporation of a pentane solution. When ethanol (4 equiv) is used instead of benzyl alcohol, the same product was obtained in lower yield (12.5 mg from 30.4 mg, 44% yield). The same product **2** can be obtained if <sup>t</sup>BuOK (2 equiv) is used as a base instead of NaH. NMR spectra of the product match those for previously reported and characterized **2** obtained by a different method.<sup>19</sup> <sup>31</sup>P{<sup>1</sup>H} NMR (C<sub>6</sub>D<sub>6</sub>, 500 MHz): 74.58 ppm (calibrated against H<sub>3</sub>PO<sub>4</sub> external reference). <sup>1</sup>H NMR (C<sub>6</sub>D<sub>6</sub>, 500 MHz): −20.58 (t, 1H, *J* = 22 Hz, RuH), 0.68 (vq, 6H, *J*<sub>HP</sub> = 13.5 Hz, *J*<sub>HH</sub> = 6.8 Hz, PCH(CH<sub>3</sub>)<sub>2</sub>), 0.98 (vq, 6H, *J*<sub>HP</sub> = 13.9 Hz, *J*<sub>HH</sub> = 6.9 Hz, PCH(CH<sub>3</sub>)<sub>2</sub>), 1.15 (vq, 6H, *J*<sub>HP</sub> = 13.6 Hz, *J*<sub>HH</sub> = 6.8 Hz, PCH(CH<sub>3</sub>)<sub>2</sub>); 1.22 (vq, 6H, *J*<sub>HP</sub> = 15.1 Hz, *J*<sub>HH</sub> = 7.1 Hz, PCH(CH<sub>3</sub>)<sub>2</sub>), 1.44–1.56 (m, 2H, PCH(CH<sub>3</sub>)<sub>2</sub>), 1.90–2.03 (m, 2H, PCH(CH<sub>3</sub>)<sub>2</sub>), 2.49–2.60 (m, 2H, PCHH), 2.92 (d, 2H, *J*<sub>PH</sub> = 12.5 Hz, PCHH), 3.54 (d, 1H, *J*<sub>HH</sub> = 14.3 Hz, acridine C<sub>9</sub>HH), 3.72 (d, 1H, *J*<sub>HH</sub> = 14.3 Hz, acridine C<sub>9</sub>HH), 6.8–7.0 (m, 4H, aryl), 7.10–7.25 (m, 2H, overlaps with solvent peak). <sup>13</sup>C{<sup>1</sup>H} NMR (C<sub>6</sub>D<sub>6</sub>, 500 MHz): 17.6 (s, PCH(CH<sub>3</sub>)<sub>2</sub>), 18.7 (s, PCH(CH<sub>3</sub>)<sub>2</sub>), 19.2 (s, PCH(CH<sub>3</sub>)<sub>2</sub>), 20.4 (s, PCH(CH<sub>3</sub>)<sub>2</sub>), 24.3 (t, *J*<sub>CP</sub> = 7.8 Hz, PCH(CH<sub>3</sub>)<sub>2</sub>), 25.7 (t, *J*<sub>CP</sub> = 14.9 Hz, PCH(CH<sub>3</sub>)<sub>2</sub>), 27.9 (t, *J*<sub>CP</sub> = 9.2 Hz, PCH<sub>2</sub>). 36.5 (s, acridine C<sub>9</sub>), 119.3 (s, Ar), 121.7 (s, Ar, quat), 126.6 (s, Ar), 128.3 (s, Ar), 153.1 (t, *J*<sub>CP</sub> = 4.5 Hz, Ar, quat), 210.1 (s, CO).

**General Procedure for Pyrrolidine-to-Pyrrolidone Conversion Catalyzed by 2.** A 50 mL pressure tube equipped with a magnetic stirring bar was charged under N<sub>2</sub> atmosphere with a solution of 0.010 mmol of **2** in 1.5 mL of dioxane, 1.5 mL of distilled water, and 1 mmol of pyrrolidine. The reaction mixture was stirred and heated in a Teflon-sealed tube at 150 °C silicon bath temperature. After 48 h, the reaction mixture was cooled down, an internal standard (20 μL of pyridine) was added, and the reaction mixture was analyzed by NMR. For NMR analysis, a sample of the reaction mixture (30–50 μL) was dissolved in 0.5–0.6 mL of D<sub>2</sub>O and analyzed by <sup>1</sup>H NMR. The crude yields were determined by <sup>1</sup>H NMR by integration vs pyridine internal standard; long delay time (10 s) was used to quantify the amount of products. Characterization of the products was reported previously.<sup>13</sup> **WARNING!** Pressure develops during the reaction in a closed system due to H<sub>2</sub> evolution and significant solvent vapor pressure at high temperatures. All reactions should be performed in thick-glass pressure tubes using proper shielding. The reaction mixtures should be cooled down in ice bath before slowly releasing the H<sub>2</sub> gas formed.

**X-ray Structure Determinations of 2.** Crystal data: C<sub>28</sub>H<sub>41</sub>N<sub>1</sub>O<sub>1</sub>P<sub>2</sub>Ru<sub>1</sub>, orange, 0.03 × 0.12 × 0.14 mm<sup>3</sup>, orthorhombic, *P*2<sub>1</sub>2<sub>1</sub>2<sub>1</sub>, *a* = 11.2347(18) Å, *b* = 12.603(3) Å, *c* = 18.665(4) Å from 20° of data, *T* = 100(2) K, *V* = 2642.7(9) Å<sup>3</sup>, *Z* = 4, *F*<sub>w</sub> = 570.63, *D*<sub>c</sub> = 1.434 Mg·m<sup>−3</sup>, *μ* = 0.736 mm<sup>−1</sup>. Data collection and processing: Bruker Apex2 KappaCCD diffractometer, MoKα (*λ* = 0.71073 Å), graphite monochromator, 15569 reflections collected, −14 ≤ *h* ≤ 11, −15 ≤ *k* ≤ 15, −16 ≤ *l* ≤ 23, frame scan width = 0.5°, scan speed 1° per 240 s, typical peak mosaicity 0.69°, 5495 independent reflections (*R*-int = 0.0297). The data were processed with Denzo-Scalepack. Solution and refinement: structure solved by direct methods with ShelxT. Full matrix least-squares refinement based on *F*<sup>2</sup> with SHELXL-97. 310 parameters with 0 restraints, final *R*<sub>1</sub> = 0.0264 (based on *F*<sup>2</sup>) for data with *I* > 2σ(*I*) and *R*<sub>1</sub> = 0.0317 on 5495 reflections, goodness-of-fit on *F*<sup>2</sup> = 1.048, largest electron density peak = 0.419 Å<sup>−3</sup>, deepest hole −0.426 Å<sup>−3</sup>. Position of hydrogen H1 was localized as an electron density peak. Positional and isotropic temperature



parameters of H1 were varied during last 10 cycles of refinement together with parameters of other atoms.

**Computational Details.** All geometries were optimized with the BP86 functional and the def2-SV(P) basis set together with corresponding core potential for ruthenium. The D3 dispersion correction was used for the geometry optimizations. Thermodynamic properties were obtained at the same level of theory from a frequency calculation. All free energies are calculated under standard conditions unless otherwise noted. Single point energies were obtained with the dispersion corrected, spin scaled double hybrid functional DSD-PBEB95-D3BJ together with a larger def2-TZVPP basis set. In order to increase the efficiency of the calculations, the density fitting, respectively, the RIJOSX approximation with the approximate basis sets was used. To take the influence of the solvent into account, the SMD model was applied for a 1:1 mixture of dioxane/water. The geometry optimizations were performed with Gaussian 09, whereas the double-hybrid single point calculations utilized the ORCA program package.<sup>31,32</sup>

## ■ ASSOCIATED CONTENT

### Supporting Information

Experimental details of synthetic procedures, catalytic reactions, and computational details. This material is available free of charge via the Internet at <http://pubs.acs.org>.

## ■ AUTHOR INFORMATION

### Corresponding Author

\*[david.milstein@weizmann.ac.il](mailto:david.milstein@weizmann.ac.il)

### Present Address

§Okinawa Institute of Science and Technology Graduate University, 1919-1 Tancha, Onna-son, Kunigami-gun, Okinawa, Japan 904-0495

### Author Contributions

‡These authors contributed equally.

### Notes

The authors declare no competing financial interest.

## ■ ACKNOWLEDGMENTS

This research was supported by the European Research Council under the FP7 framework (ERC no. 246837), the Israel Science Foundation and the Kimmel Center for Molecular Design. J.R.K. thanks the Feinberg Graduated School for a Post Doctoral Fellowship. U.G. thanks the DAAD for a Post Doctoral Fellowship. D.M. holds the Israel Matz Professorial Chair of Organic Chemistry.

## ■ REFERENCES

- (1) Rees, C. W.; Meth-Cohn, O.; Katritzki, A. R.; Moody, C. J. *Comprehensive Organic Functional Group Transformations, Vol. 5, Synthesis: Carbon with Two Attached Heteroatoms with at Least One Carbon-to-Heteroatom Multiple Link*; Pergamon: Oxford, UK, 1995.
- (2) Naota, T.; Murahashi, S. *Synlett* **1991**, 693.
- (3) Gunanathan, C.; Ben-David, Y.; Milstein, D. *Science* **2007**, *317*, 790.
- (4) Moriarty, R. M.; Vaid, R. K.; Duncan, M. P.; Ochiai, M.; Inenaga, M.; Nagao, Y. *Tetrahedron Lett.* **1988**, *29*, 6913.
- (5) Wu, X.-F.; Sharif, M.; Pews-Davtyan, A.; Langer, P.; Ayub, K.; Beller, M. *Eur. J. Org. Chem.* **2013**, *2013*, 2783.
- (6) Wu, X.-F.; Sharif, M.; Feng, J.-B.; Neumann, H.; Pews-Davtyan, A.; Langer, P.; Beller, M. *Green Chem.* **2013**, *15*, 1956.
- (7) Wu, X.-F.; Bheeter, C. B.; Neumann, H.; Dixneuf, P. H.; Beller, M. *Chem. Commun.* **2012**, *48*, 12237.
- (8) Wang, Y.; Kobayashi, H.; Yamaguchi, K.; Mizuno, N. *Chem. Commun.* **2012**, *48*, 2642.
- (9) Xu, W.; Jiang, Y.; Fu, H. *Synlett* **2012**, *23*, 801.

(10) Klobukowski, E. R.; Mueller, M. L.; Angelici, R. J.; Woo, L. K. *ACS Catal.* **2011**, *1*, 703.

(11) Tanaka, K.; Yoshifuji, S.; Nitta, Y. *Chem. Pharm. Bull.* **1988**, *36*, 3125.

(12) Nishinaga, A.; Shimizu, T.; Matsuura, T. *J. Chem. Soc., Chem. Commun.* **1979**, 970.

(13) Khusnutdinova, J. R.; Ben-David, Y.; Milstein, D. *J. Am. Chem. Soc.* **2014**, *136*, 2998.

(14) Gunanathan, C.; Milstein, D. *Angew. Chem., Int. Ed.* **2008**, *47*, 8661.

(15) Gunanathan, C.; Shimon, L. J. W.; Milstein, D. *J. Am. Chem. Soc.* **2009**, *131*, 3146.

(16) Khusnutdinova, J. R.; Ben-David, Y.; Milstein, D. *Angew. Chem., Int. Ed.* **2013**, *52*, 6269.

(17) Balaraman, E.; Khaskin, E.; Leitun, G.; Milstein, D. *Nat. Chem.* **2013**, *5*, 122.

(18) Rodríguez-Lugo, R. E.; Trincado, M.; Vogt, M.; Tewes, F.; Santiso-Quinones, G.; Grützmacher, H. *Nat. Chem.* **2013**, *5*, 342.

(19) Gunanathan, C.; Gnanaprakasam, B.; Iron, M. A.; Shimon, L. J. W.; Milstein, D. *J. Am. Chem. Soc.* **2010**, *132*, 14763.

(20) Ye, X.; Plessow, P. N.; Brinks, M. K.; Schelwies, M.; Schaub, T.; Rominger, F.; Paciello, R.; Limbach, M.; Hofmann, P. *J. Am. Chem. Soc.* **2014**, *136*, 5923.

(21) The previously published X-ray structure of **2** (ref 17) was obtained for single crystals grown under different crystallization conditions: this structure includes benzene from crystallization and exhibits disorder; no hydride could be located.

(22) Baker, J. D.; Heath, R. T.; Millar, J. G. *J. Chem. Ecol.* **1992**, *18*, 1595.

(23) Kesharwani, M. K.; Martin, J. M. L. *Theor. Chem. Acc.* **2014**, *133*, 1452.

(24) Since an optimization with analytical calculation of the Hessian and a stepsize of 0.01 bohr did not converge, we estimated the barrier for H<sub>2</sub> elimination from an relaxed PES scan over the H–H distance with a final stepsize of 0.01 Å.

(25) Li, J.; Shiota, Y.; Yoshizawa, K. *J. Am. Chem. Soc.* **2009**, *131*, 13584.

(26) Iron, M. A.; Ben-Ari, E.; Cohen, R.; Milstein, D. *Dalton Trans.* **2009**, 9433.

(27) Sandhya, K. S.; Suresh, C. H. *Organometallics* **2011**, *30*, 3888.

(28) Yang, X.; Hall, M. B. *J. Am. Chem. Soc.* **2010**, *132*, 120.

(29) Orlova, G.; Scheiner, S.; Kar, T. *J. Phys. Chem. A* **1999**, *103*, 514.

(30) Gottlieb, H. E.; Kotlyar, V.; Nudelman, A. *J. Org. Chem.* **1997**, *62*, 7512.

(31) Frisch, M. J.; Trucks, G. W.; Schlegel, H. B.; Scuseria, G. E.; Robb, M. A.; Cheeseman, J. R.; Scalmani, G.; Barone, V.; Mennucci, B.; Petersson, G. A.; Nakatsuji, H.; Caricato, M.; Li, X.; Hratchian, H. P.; Izmaylov, A. F.; Bloino, J.; Zheng, G.; Sonnenberg, J. L.; Hada, M.; Ehara, M.; Toyota, K.; Fukuda, R.; Hasegawa, J.; Ishida, M.; Nakajima, T.; Honda, Y.; Kitao, O.; Nakai, H.; Vreven, T.; Montgomery, J. A., Jr.; Peralta, J. E.; Ogliaro, F.; Bearpark, M.; Heyd, J. J.; Brothers, E.; Kudin, K. N.; Staroverov, V. N.; Kobayashi, R.; Normand, J.; Raghavachari, K.; Rendell, A.; Burant, J. C.; Iyengar, S. S.; Tomasi, J.; Cossi, M.; Rega, N.; Millam, N. J.; Klene, M.; Knox, J. E.; Cross, J. B.; Bakken, V.; Adamo, C.; Jaramillo, J.; Gomperts, R.; Stratmann, R. E.; Yazyev, O.; Austin, A. J.; Cammi, R.; Pomelli, C.; Ochterski, J. W.; Martin, R. L.; Morokuma, K.; Zakrzewski, V. G.; Voth, G. A.; Salvador, P.; Dannenberg, J. J.; Dapprich, S.; Daniels, A. D.; Farkas, Ö.; Foresman, J. B.; Ortiz, J. V.; Cioslowski, J.; Fox, D. J. *Gaussian 09*, revision D1; Gaussian, Inc: Wallingford, CT, 2009.

(32) Neese, F. *WIREs Comput. Mol. Sci.* **2012**, *2*, 73.